

Deadbeat Predictive Control Method for 4-leg Inverters

Tuhin Ibrahim Khan^{1*}, Hai Tung Luu¹, Laszlo Szamel¹

¹ Department of Electric Power Engineering, Faculty of Electrical Engineering and Informatics, Budapest University of Technology and Economics, Egry József u. 18., H-1111 Budapest, Hungary

* Corresponding author, e-mail: tuhin27mar@edu.bme.hu

Received: 10 August 2022, Accepted: 22 September 2022, Published online: 27 October 2022

Abstract

Until now, computational burden alleviation and stability issues for the three-phase four-leg converter has not yet been thoroughly investigated. However, compared to the conventional controllers, the implementation of predictive current control approach for 3- \emptyset , 4-L inverter suffers a large computational burden due to its additional fourth-leg. Motivated by this fact, this article provides an alternative predictive current control implementation for 3- \emptyset , 4-L inverter which offers reduced computational effort to achieve similar performance as the conventional FCS-MPC and ensures the global stability of the closed-loop system. To further understand the consequences of the developed control law, theoretical stability analysis has been carried out that links Lyapunov's direct method with the closed-loop system behavior. The outcome of the theoretical stability analysis demonstrates the global stability of the overall system which is later supported by the experimental results. With the proposed method, the number of possible voltage vectors required to obtain the optimal voltage vector in each sampling interval reduces from sixteen to five and thereby simplifies the prediction process. It is also derived that the Lyapunov function-based approach actually yields to the dead-beat control, which has not been previously highlighted in the previous papers. The current work also provides experimental results for different loading conditions (balanced and unbalanced) which further demonstrates the efficacy of the proposed method.

Keywords

deadbeat, FCS-MPC, Lyapunov function, predictive current control, inverters

1 Introduction

3- \emptyset , 4-L voltage source inverters are one of the most popular choices for forming distributed generation systems and ac microgrids [1, 2] (Fig. 1). The 3- \emptyset , 4-L voltage source inverters also provide flexible solutions for different other power electronics applications that include active power filtering, nonlinear load harmonics and imbalances compensation, grid power quality improvement, fault tolerant operation of drives, UPS (uninterruptible power supply) applications [3–7] and so on. However, for distributed generation systems, the role of the 3- \emptyset , 4-L inverter is mostly to ameliorate the poor power quality issues due to intermittent nature of renewable energy sources which includes the lower power factor, distorted dc voltage, and higher current ripple [8]. Thus, the control technique of the 3- \emptyset , 4-L inverter needs to consider two important aspects that include stability and efficiency.

By now the basic control concept for this converter is widely known and well understood. There are examples of implementation of various modulation schemes for 3- \emptyset , 4-L inverter. Several types of advanced control schemes

such as the selective harmonic elimination (SHE) [9], carrier-based sinusoidal pulse width modulation (SPWM) [10], and 3-D space vector modulation (3-D-SVM) [11] methods have already applied to 3- \emptyset , 4-L inverters. However, these control schemes suffer some drawbacks such as complexity, steady-state error, and sensitivity to parameter uncertainty [12, 13]. Recently, a sliding mode controller is presented which regulates the output voltage of the four-legged inverter featuring fixed switching frequency operation [12]. The proposed method can reduce the chattering problem significantly without affecting the robustness, regulation and dynamic response. A new deadbeat controller is proposed in [13] which employs a discrete-time control platform for achieving the fastest possible dynamic performance. Predictive control is another class of controller which is gaining popularity in recent times among the industrial communities due to its simplicity, improved dynamics, and the inclusion of several non-linear constraints in the cost function [14–19]. Like other power converters, several FCS-MPC implementations have already

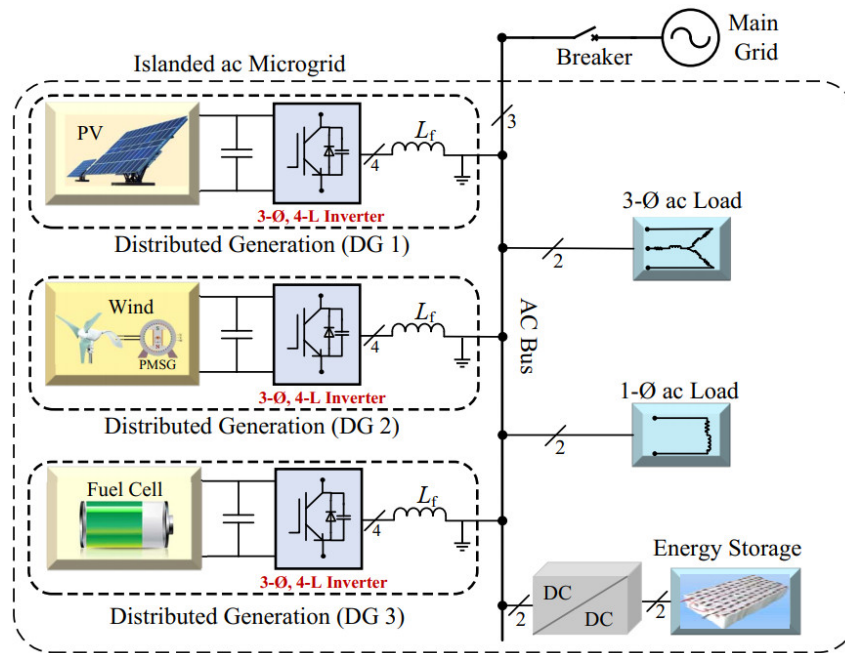


Fig. 1 A schematic ac microgrid structure with distributed generation systems

been reported for 3-Ø, 4-L inverters till now. In [14] a predictive control approach is presented to control the load current of 3-Ø, 4-L inverters using a predictive cost function without any modulation stage. However, there is a lack of discussions addressing the stability issues and the reduction of computational burden.

Two-step prediction-based FCS-MPC is proposed in [15] which can improve the performance of the converter concerning the load voltage quality. Besides, switching frequency reduction is highlighted. In [3] a model predictive control for the 3-Ø, 4-L inverters with grid interfacing capability is presented with an advanced controller (combination of FPGA and DSP) to reduce the computation time. Although a great variety of predictive control approach has been presented for this inverter, quite limited number of research works exist in the literature which demonstrates the stability and parameter independence of the FCS-MPC controlled 3-Ø, 4-L inverter.

The closed-loop stability of the FCS-MPC is usually investigated by using Lyapunov's direct method. Lyapunov's direct method has been proven to be a useful and reliable tool for investigating the stability of the power converters [20]. Various approaches to Lyapunov function-based methods that play a vital role in both stability analysis and control synthesis for nonlinear dynamical systems are already highlighted in [21–24]. Some other notable contributions involving the Lyapunov function-based control method for an exponentially stable closed-loop system is reviewed in [25–28].

Besides, the implementation of FCS-MPC for 3-Ø, 4-L inverter often faces the unavoidable computational burden. This heavy computational load is due to the additional fourth leg [13] in its configuration. Thus, it is desirable to develop a specialized FCS-MPC algorithm for 3-Ø, 4-L inverter that requires a minimal number of calculations. In summary, some important aspects of FCS-MPC such as closed-loop stability and computational burden alleviation have not been studied in depth for four-legged inverters. Motivated by the above-mentioned research gap, this paper proposes a modified FCS-MPC algorithm for 3-Ø, 4-L inverter to ensure global stability and reduce the unavoidable computational difficulties placed on the controller. For the current work, it has been mathematically proven that all signals of the closed-loop dynamics of the proposed system are uniformly and ultimately bounded. Experimental results included in this paper clearly demonstrate the stability and the computation time reduction mentioned above.

This article is structured to present in Section 2 the topological structure of the 3-Ø, 4-L inverter. Section 3 describes the formulation of the proposed FCS-MPC algorithm. Section 4 is exclusively dedicated to highlighting the advantages of the proposed scheme in comparison to the conventional approach. Moreover, the experimental results are presented in Section V. Finally, the conclusion is drawn in Section 6.

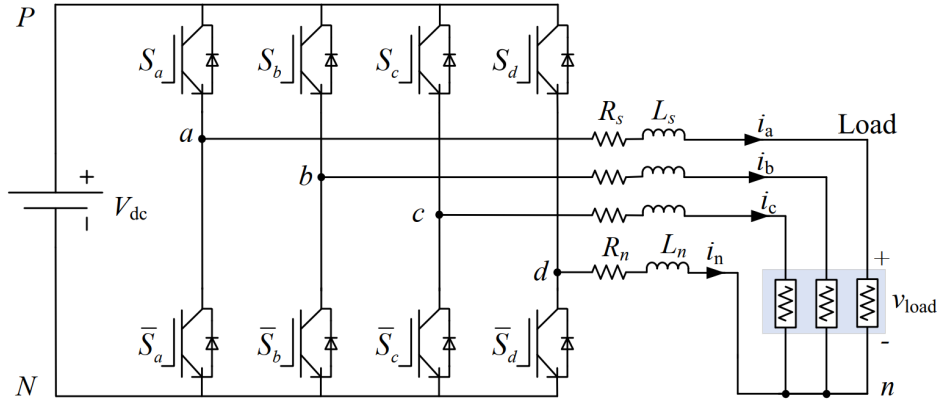


Fig. 2 Two-level 3-Ø, 4-L inverter topology

2 The 3-Ø, 4-L inverters system configuration

Fig. 2 shows the basic circuit topology of the 3-Ø, 4-L inverter system. The three-legs of this inverter is connected to the loads through L filters as shown in Fig. 2. The zero-sequence path is created between the fourth-leg of the inverter and the neutral point of the load via an inductor.

To simplify the analysis, the following vectors are adopted:

$$\begin{aligned} \mathbf{u}_{inv} &= [\mathbf{u}_{an} \quad \mathbf{u}_{bn} \quad \mathbf{u}_{cn}]^T, \\ \mathbf{v}_{load} &= [\mathbf{v}_{an} \quad \mathbf{v}_{bn} \quad \mathbf{v}_{cn}]^T, \\ \mathbf{i} &= [\mathbf{i}_a \quad \mathbf{i}_b \quad \mathbf{i}_c]^T, \end{aligned} \quad (1)$$

where \mathbf{u}_{inv} represents the converter voltage/actuation voltage, \mathbf{v}_{load} is the voltages across the loads, and \mathbf{i} is the three-phase load current. Referring to Fig. 2, the dynamic equation which represents the converter characteristic can be expressed as:

$$\mathbf{u}_{inv} = \mathbf{R}_s \mathbf{i} + \mathbf{L}_s \frac{d\mathbf{i}}{dt} + \mathbf{v}_{load} + \mathbf{v}_{Ln}, \quad (2)$$

where, the inductance of the filter components is represented by \mathbf{L}_s . \mathbf{R}_s represents the leakage resistance and \mathbf{L}_n is the neutral inductance to limit the ripple of the neutral current.

The discretized version of Eq. (2) using Euler's approach can be written as:

$$\mathbf{u}_{inv}[k] = \mathbf{R}_s \mathbf{i}[k] + \mathbf{L}_s \frac{\mathbf{i}[k+1] - \mathbf{i}[k]}{T_s} + \mathbf{v}_{load}[k] + \mathbf{v}_{Ln}[k]. \quad (3)$$

The predicted current vector flowing through the filter component L is calculated using the discrete-time domain derived from Eq. (3):

$$\mathbf{i}[k+1] = \mathbf{i}[k] + \frac{T_s}{L_s} \{ \mathbf{u}_{inv}[k] - \mathbf{v}_{Ln}[k] - \mathbf{v}_{load}[k] \}. \quad (4)$$

The voltage across neutral point inductor (\mathbf{v}_{Ln}) can be estimated as:

$$\begin{aligned} \mathbf{v}_{Ln}[k] &= \frac{L_n}{T_s} [\{ \mathbf{i}_a[k] - \mathbf{i}_a[k-1] \} \\ &\quad + \{ \mathbf{i}_b[k] - \mathbf{i}_b[k-1] \} + \{ \mathbf{i}_c[k] - \mathbf{i}_c[k-1] \}]. \end{aligned} \quad (5)$$

The 3-Ø, 4-L inverter voltage vectors can be generalized using a simple mathematical equation which relates the measured dc-bus voltage and the converter switching states as indicated below:

$$\mathbf{u}_{inv}[k] = \begin{bmatrix} \mathbf{u}_{an}[k] \\ \mathbf{u}_{bn}[k] \\ \mathbf{u}_{cn}[k] \end{bmatrix} = \begin{bmatrix} (\mathcal{S}_{a1} - \mathcal{S}_{d1})V_{dc}[k] \\ (\mathcal{S}_{b1} - \mathcal{S}_{d1})V_{dc}[k] \\ (\mathcal{S}_{c1} - \mathcal{S}_{d1})V_{dc}[k] \end{bmatrix}, \quad (6)$$

where \mathcal{S}_{a1} , \mathcal{S}_{b1} , \mathcal{S}_{c1} , and \mathcal{S}_{d1} are the switching states of the converter (\mathcal{S}_{a1} , \mathcal{S}_{b1} , \mathcal{S}_{c1} , and \mathcal{S}_{d1} represents the on-state of the switches while \mathcal{S}_{a2} , \mathcal{S}_{b2} , \mathcal{S}_{c2} , and \mathcal{S}_{d2} represents off-state of the switches). The switching states \mathcal{S}_{a1} , \mathcal{S}_{b1} , \mathcal{S}_{c1} , and \mathcal{S}_{d1} form sixteen possible combinations and those sixteen switching combinations are used in the cost function minimizing the process of the FCS-MPC algorithm. The tips of these sixteen voltage vectors when projected onto the α - β frame form a regular hexagon as shown in Fig. 3.

3 Control problem formation

3.1 Control objective

The primary control goal of the 3-Ø, 4-L inverter is to minimize its energy losses due to poor current tracking and higher THD in AC-current. For ensuring the proper operation of the 3-Ø, 4-L inverter, the primary control goal of the 3-Ø, 4-L inverter is to minimize its energy losses due to poor current tracking and higher THD in AC-current. For ensuring the proper operation of the 3-Ø, 4-L inverter and must confine the currents within its maximum limit.

$$\vec{\mathbf{i}}_{min} < \vec{\mathbf{i}}(t) < \vec{\mathbf{i}}_{max} \quad (7)$$

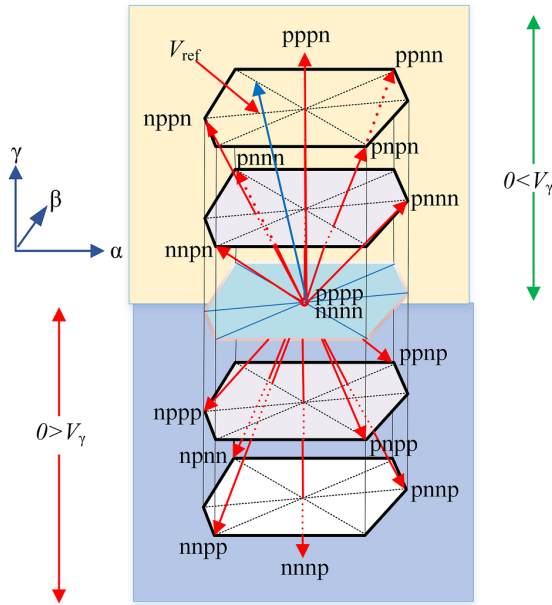


Fig. 3 Space vector diagram of the three-phase four-legged inverter topology

3.2 Conventional approach

To improve the current tracking, the conventional FCS-MPC algorithm firstly calculates the future current ($i[k+1]$) for each possible voltage (u_{inv}) of the 3- ϕ , 4-L inverter. This voltage vector can be determined directly from the inverter switching states by using Eq. (6). Then, the voltage vector which minimizes the cost function is applied to the inverter to achieve desired control output. This control technique produces a significant amount of calculation burden to the FCS-MPC algorithm [13] for controlling the three-phase current. This large number of calculation burden can be reduced by considering the inverter voltage (u_{inv}) as a control variable which will be shown later in this paper. For the conventional approach the cost-function can be written as [14]:

$$g[k+2] = \left[i[k]^* - i[k+2] \right]. \quad (8)$$

Here, current ($i[k+2]$) is considered for delay compensation purpose. Then, the MPC algorithm compares the numerical values of Eq. (8) for different switching states and subsequently selects the optimal switching state which gives the minimum value in Eq. (8).

3.3 Proposed approach

From the control point of view, an optimizer selects the optimal converter switching states for the cost function minimization where the prediction variable is linked with the dynamic model of the 3- ϕ , 4-L inverter. This optimization is achieved by extensively searching all possible converter switching states.

The primary goal of the proposed method is to utilize a modified digital predictive current control scheme to reduce the computational effort of the controller. Overall, the idea is to avoid the sixteen current predictions in the current prediction loop. Besides, the stability issues will also be investigated using Lyapunov's stability theory. For the present analysis, the control law to satisfy the control objective of Eq. (7) or to control the dynamics of the load current is chosen as:

$$u_{inv}^*[k+1] = -\frac{L_s}{T_s} i[k] + \frac{R_s T_s + L_s}{T_s} i^*[k+1] + v_{load}[k] + v_{Ln}[k]. \quad (9)$$

The proposed approach features the calculation of the desired inverter output voltage $u_{inv}^*[k+1]$ reference. From Eq. (9), it can be said that the load current will be exactly equal to its reference value when the converter voltage vector chosen by the controller will be same as $u_{inv}^*[k+1]$. However, this may not be possible at all times. The reason for this is the finite control actions/ lack of modulation approach in FCS-MPC and for the case of four-legged inverters, the control actions are limited by the sixteen combinations of switching state. However, even if the exact voltage vector is not selected, the one closest to that can be selected and the conditions stated by Eq. (4) will be satisfied. Thus, the control actions will still be the most appropriate. In summary, the cost function with the proposed approach becomes:

$$J[k+1] = \left[u_{inv}^*[k+1] - u_{inv}[k+1] \right]. \quad (10)$$

4 Advantages compared to the conventional approach

4.1 Global stability

Lyapunov's stability theory is a widely used method to investigate the stability of a non-linear system. The stability phenomenon is similar to the energy behavior of any electrical system. Say for example, in an electrical system the energy is stored in the capacitors/inductors and dissipated through the resistive elements. Thus, the total energy consumption is balanced, and the total system of the system eventually decays to zero. A similar concept is followed in the Lyapunov's stability theory. If a practical control Lyapunov function exists for a system for which the total energy of that system converges to zero, then the system is said to be globally stable.

This leads to the definition of the practical control Lyapunov function (CLF) as discussed in [29]. In the following part, it will be proven mathematically that the proposed control technique can ensure the global stability.

The stability analysis starts with the definition of the load current error (\mathbf{i}_{err}) of the 3- \emptyset , 4-L inverter. This load current error for the inverter can be represented as:

$$\mathbf{i}_{err}[k+1] = \mathbf{i}^*[k+1] - \mathbf{i}[k+1]. \quad (11)$$

The future current error in the discrete form can be expressed as:

$$\mathbf{i}_{err}[k+1] = \frac{1}{\mathbf{R}_s \mathbf{T}_s} (\mathbf{L}_s \mathbf{i}[k] + \mathbf{T}_s \mathbf{u}_{inv}[k] - \mathbf{T}_s \mathbf{v}_{load}[k] - \mathbf{T}_s \mathbf{v}_{Ln}[k]) - \mathbf{i}^*[k+1]. \quad (12)$$

To control the dynamics of the load current control law is chosen as Eq. (9). The dynamics of the load current controlled by Eq. (9) will be globally stable for the following set:

$$\sigma = \left\{ \mathbf{i}_{err} \mid \mathbf{i}_{err} \leq \left(\frac{\mathbf{T}_s}{\mathbf{R}_s \mathbf{T}_s + \mathbf{L}_s} \right) (\boldsymbol{\Psi} + \epsilon) \right\}, \quad (13)$$

where, $\boldsymbol{\Psi}$ and ϵ are the constants and represents the upper bound of the errors associated with the quantization and estimation process of the load voltage. The solutions of the current tracking dynamics are asymptotically stable if an input such that $\mathbf{i}_{err}[k] \in \mathbf{G}$ and a control Lyapunov function $V(\mathbf{i}_{err}[k])$ exists which satisfies the following inequality:

$$\begin{aligned} V(\mathbf{i}_{err}[k+1]) - V(\mathbf{i}_{err}[k]) &\geq \mathbf{L}_{c1} \mathbf{i}_{err}[k+1] - \mathbf{i}_{err}[k], \\ \forall \mathbf{u}_{err}[k] &\in A; \\ V(\mathbf{i}_{err}[k+1]) - V(\mathbf{i}_{err}[k]) &\leq \mathbf{L}_{c2} \mathbf{i}_{err}[k+1] - \mathbf{i}_{err}[k]^l, \\ \forall \mathbf{u}_{err}[k] &\in \gamma; \\ \Delta V(\mathbf{u}_{err}[k]) &< -\mathbf{L}_{c3} \|\mathbf{i}_{err}[k]\|^l + \mathbf{L}_{c4}, \end{aligned} \quad (14)$$

where, \mathbf{L}_{c1} to \mathbf{L}_{c4} are positive constants. $1 \leq l$. $A \subseteq \mathbf{R}^n$ represents an invariant control set which is positive while $\gamma \subset \mathbf{R}^n$ represents a compact set. For the present analysis, the future voltage vector is related with the converter voltage vectors at $(k+1)$ sampling period and the quantization error. This can be expressed as Eq. (15):

$$\mathbf{u}_{inv}[k+1] = \bar{\mathbf{u}}_{inv}[k+1] + \Delta[k+1]. \quad (15)$$

$\Delta[k+1]$ in Eq. (15) stands for the error associated with the quantization process and $\bar{\mathbf{u}}_{inv}[k+1]$ is the continuous voltage input vector. $\Delta[k+1]$ satisfies the following condition:

$$|\Delta(k+1)| \leq \boldsymbol{\Psi} (\boldsymbol{\Psi} > 0) \quad (16)$$

where, $\boldsymbol{\Psi}$ is the upper bound of the quantization error.

For assessing the global stability, a Lyapunov function (LF) can be defined as:

$$V(\mathbf{i}_{err}[k]) = \frac{1}{2} \mathbf{i}_{err}[k]^T \mathbf{i}_{err}[k]. \quad (17)$$

Using Eq. (12) and Eq. (17), the change of the Lyapunov function can be expressed as:

$$\Delta V[k] = V(\mathbf{i}_{err}[k+1]) - V(\mathbf{i}_{err}[k]). \quad (18)$$

Using Eq. (11), Eq. (18) can be written as:

$$\Delta V(\mathbf{i}_{err}[k]) = \frac{1}{2} \left(\frac{1}{\mathbf{R}_s \mathbf{T}_s + \mathbf{L}_s} \left\{ \begin{array}{l} \mathbf{L}_s \mathbf{i}[k] + \mathbf{T}_s \mathbf{u}_{inv}[k+1] + \mathbf{T}_s \Delta[k+1] \\ -\mathbf{T}_s \mathbf{v}_{load}[k+1] + \mathbf{T}_s \hat{\mathbf{v}}_{load}[k] - \mathbf{T}_s \mathbf{v}_{Ln}[k] \end{array} \right\} - \mathbf{i}^*[k+1]^T \right) \left(\frac{1}{\mathbf{R}_s \mathbf{T}_s + \mathbf{L}_s} \left\{ \begin{array}{l} \mathbf{L}_s \mathbf{i}[k] + \mathbf{T}_s \mathbf{u}_{inv}[k+1] + \mathbf{T}_s \Delta[k+1] \\ -\mathbf{T}_s \mathbf{v}_{load}[k+1] + \mathbf{T}_s \hat{\mathbf{v}}_{load}[k] - \mathbf{T}_s \mathbf{v}_{Ln}[k] \end{array} \right\} - \mathbf{i}^*[k+1] \right) - \frac{1}{2} \mathbf{i}_{err}[k]^T \mathbf{i}_{err}[k]. \quad (19)$$

Here, the converter voltage vector, $\mathbf{u}_{inv}[k+1]$ is a finite set and bounded. The other terms in Eq. (19), load currents $\mathbf{i}[k]$, load voltage and neutral inductor voltage are also bounded. Quantization error term is also bounded according to Eq. (16). This leads to the ultimate bound-

$$\Delta V[k] \leq -\frac{1}{2} \mathbf{i}_{err}[k]^T \mathbf{i}_{err}[k] + \left(\frac{\mathbf{T}_s}{\mathbf{R}_s \mathbf{T}_s + \mathbf{L}_s} \right)^2 (\boldsymbol{\Psi} + \epsilon)^2. \quad (20)$$

ness of the current control error to a compact set, where $\mathbf{i}_{err}[k] \in \Gamma \subset \mathbf{R}^2$. Γ is the compact set determined by the converter voltage vector and the bounded AC load current reference. Thus, Eq. (19) can be written as:

Conditions that satisfy the stability condition is as followed:

$$\mathbf{L}_{c1} = \mathbf{L}_{c2} = 1, \quad \mathbf{L}_{c3} = \frac{1}{2}, \quad (21)$$

$$\mathbf{L}_{c4} = \left(\frac{\mathbf{T}_s}{\mathbf{R}_s \mathbf{T}_s + \mathbf{L}_s} \right)^2 (\boldsymbol{\Psi} + \epsilon)^2. \quad (22)$$

This implies the convergence of the system energy to zero or convergence of the current control error in a compact set as:

$$\sigma = \left\{ \mathbf{i}_{err} \mid \mathbf{i}_{err} \leq \sqrt{\frac{\mathbf{L}_{c4}}{\mathbf{L}_{c3}}} \right\}. \quad (23)$$

Thus, according to the Lyapunov's stability criterion, the converter is asymptotically stable which implies to the continuous dissipation of the system's total energy. As entioned

earlier, the finite control set actions will limit the selection of exact converter voltage vectors as derived from Eq. (9). It is to be mentioned that, for the stability analysis effect of quantization error has been already considered.

It is worthy to mention that the control law derived from the Lyapunov function actually yields to the computation of the reference converter voltage vector. This is actually dead-beat predictive control. Thus, it is confirmed that the Lyapunov function based predictive control actually yields to dead-beat predictive control.

4.2 Computational burden reduction

Fig. 4 illustrates the geographical distribution of the inverter voltage vectors. The proposed control scheme predicts the voltage vectors in the optimization loop and the one closest to the desired voltage vector obtained by Eq. (10) is selected for control action. One of the main drawbacks of the classical approach is the high computational delay which is already reviewed in [12–13] and also discussed in the previous section.

Interestingly, the proposed approach allows preselecting the converter voltage vectors which are used for the cost-function minimization process. The reduction of admissible voltage vectors for the prediction process involves two-steps as described below.

- **Prism Identification:** This approach takes advantage of the α - β projection of the desired voltage vectors first to identify the sector as shown in Fig. 4. The identification of the sector is similar to the identification of the prism of 3D-SVM technique for four-leg inverter control [11].
- **Polarity Checking/ Tetrahedron Selection:** Once the sector is identified then the polarity detection allows to preselect five converter switching states (referred to Table 1) for cost function minimization. It can be seen that the four-combinations of the voltage polarities corresponds to the four-tetrahedrons in the space vector diagram of the four-leg inverter [11].

Firstly, the prism is identified using the α - β projection of the reference voltage vector (similar to sector identification in 2D-space vector diagram). Once the prism information is determined the next step is to search the tetrahedron in which the reference vector is located. For this purpose, each prism is further subdivided into four tetrahedrons, which leads to 24 tetrahedrons (referred to Table 1). If the reference voltage vector is located in prism 1, then using the polarities of the reference voltage vector of the

converter, the desired tetrahedron can be identified. This tetrahedron corresponds to the desired reference converter voltage vector. In summary, once the sector is identified then the polarity detection allows preselecting five converter switching states (referred to Table 1) for cost

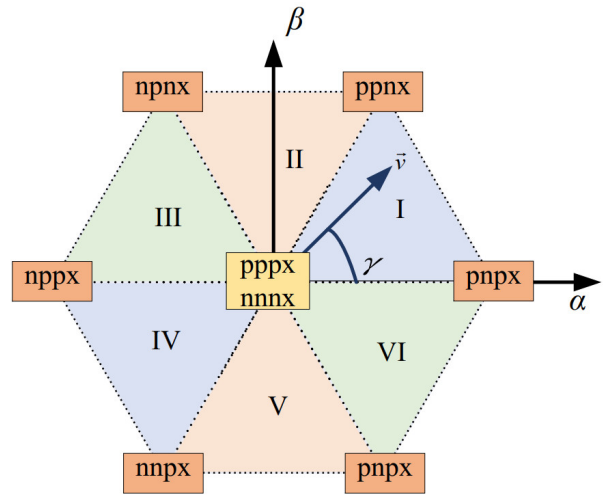


Fig. 4 α - β projection of the four-leg inverter used to identify the prism information

Table 1 Table for preselection approach

Prism	Reference Voltage Polarity	Switching States
2*1	+, -, -	pppp, nnnn, pnnp, pnpn, pppn
	+, +, -	pppp, nnnn, pnnp, pnpn, pppn
	+, +, +	pppp, nnnn, pnnp, pnpn, pppn
	+, +, +	pppp, nnnn, pnnp, pnpn, pppn
2*2	+, +, -	pppp, nnnn, pnnp, pnpn, pppn
	-, +, -	pppp, nnnn, pnnp, nppn, nppn
	+, +, +	pppp, nnnn, pnnp, nppn, nppn
	-, -, -	pppp, nnnn, pnnp, nppn, nppn
2*3	-, +, -	pppp, nnnn, nppn, nppn, nppn
	-, +, +	pppp, nnnn, nppn, nppn, nppn
	+, +, +	pppp, nnnn, nppn, nppn, nppn
	-, -, -	pppp, nnnn, nppn, nppn, nppn
2*4	-, +, +	pppp, nnnn, nppn, nppn, nppn
	-, -, +	pppp, nnnn, nppn, nppn, nppn
	+, +, +	pppp, nnnn, nppn, nppn, nppn
	-, -, -	pppp, nnnn, nppn, nppn, nppn
2*5	-, -, +	pppp, nnnn, nppn, pppn, pppn
	+, -, +	pppp, nnnn, nppn, pppn, pppn
	+, +, +	pppp, nnnn, nppn, pppn, pppn
	-, -, -	pppp, nnnn, nppn, pppn, pppn
2*6	+, -, +	pppp, nnnn, pppn, pppn, pppn
	+, -, -	pppp, nnnn, pppn, pppn, pppn
	+, +, +	pppp, nnnn, pppn, pppn, pppn
	-, -, -	pppp, nnnn, pppn, pppn, pppn

function minimization. Overall implementation process is illustrated in Fig. 4 and Fig. 5. The overall control procedure includes four main steps:

- Step-1: This step involves the load current (i) measurement along with load voltage (V_{dc}) and dc-link voltage (Vdc). The reference load current calculation (i^*) is also involved in this step.
- Step-2: This step features the reference voltage vector of the converter to track the reference load current followed by the preselection the five voltage vectors for optimization process based on Table 1.
- Step-3: Prediction of the optimal voltage vectors based on cost function minimization.
- Step-4: This step involves the application of the optimal switching states obtained from Step-3.

Fig. 6 shows a simplified block diagram concerning the overall implementation procedure of the control technique for the present work. For further clarification, the timing diagram of the proposed method is also shown in Fig. 7

The reference voltage vector for the converter will be calculated using Eq. (9). A look-up table (Table 1) will be used to choose the most appropriate control actions based on the preselection approach discussed in Section 4.2 to determine the five candidate voltage vectors to be used for the prediction process.

5 Results

The proposed control approach keeps the essence of the FCS-MPC as it uses the system model to predict the future behavior of the system variable. To prove the effectiveness

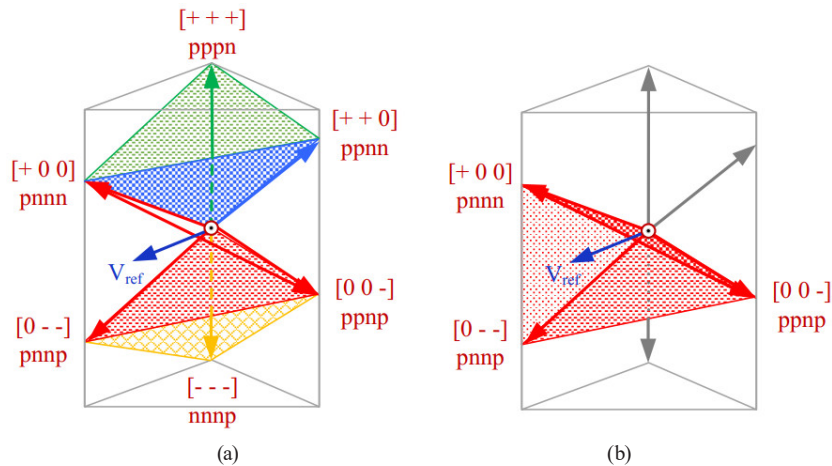


Fig. 5 (a) Prism (P1) consisting of four tetrahedrons and (b) Reference vector in tetrahedron1(T1)

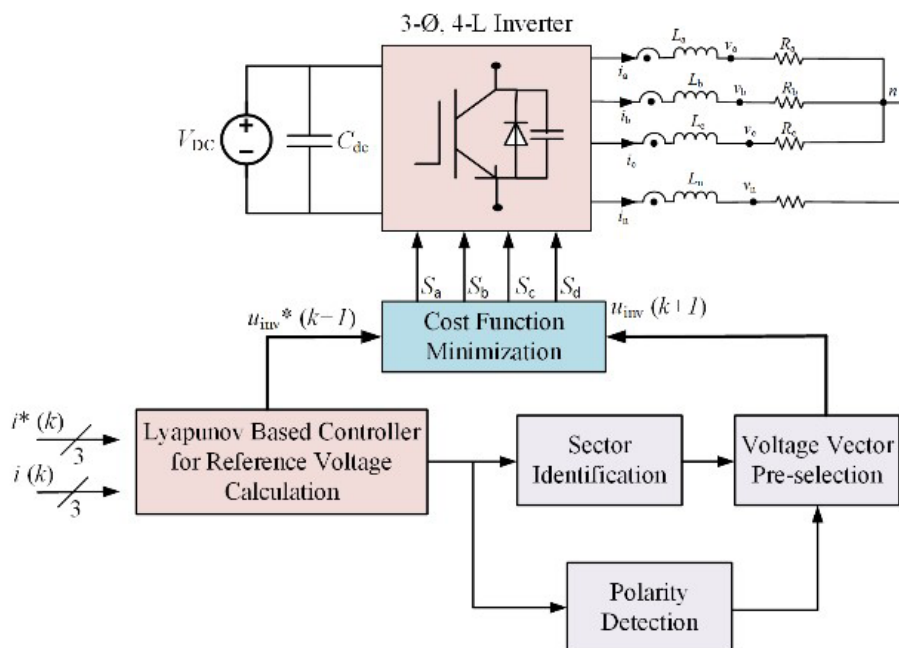


Fig. 6 Simplified block diagram of overall control block

of the developed concept, an experimental test-rig has been built as shown in Fig. 8. The setup consisted of a four-leg inverter with an insulated gate bipolar transistor (IGBT) module and a dc-link capacitor with V_{dc} equal to 200-V. Semikron IGBT modules (SKM50GB12T4) are

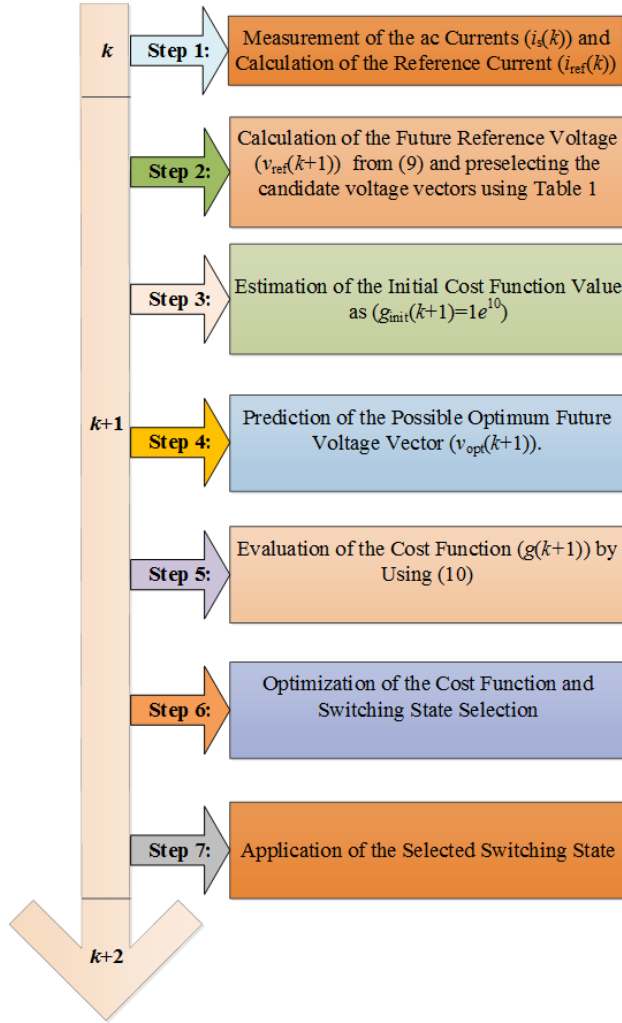


Fig. 7 Timing diagram illustration overall process

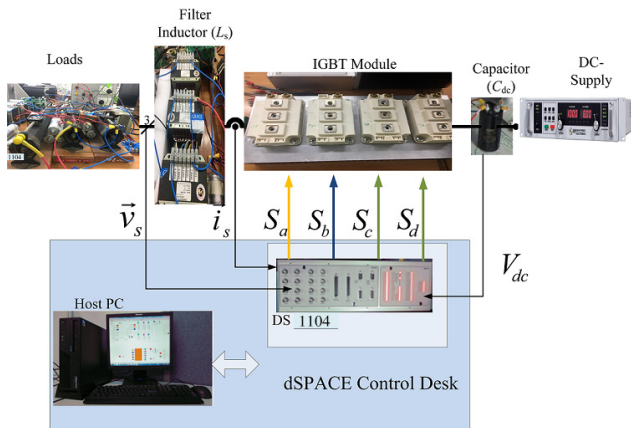


Fig. 8 Experimental set-up for 3-Ø4-L Inverter

used as the switching device. The SKYPER-32R, a Dual IGBT Driver IC, is used as an interface between IGBT modules and the controller. DS-1104 is used as the control implementation platform. All the parameters used for the experimental verification are summarized in Table 2.

5.1 Steady-state performance analysis

Different case studies are presented to demonstrate the efficacy of the present work. Measurements from experimental prototype is shown with different case studies. The following four case studies are considered in the steady-state condition:

- Case-I: balanced loads supplied with balanced reference currents.
- Case-II: unbalanced loads supplied with balanced reference currents.
- Case-III: balanced loads supplied with unbalanced reference currents.
- Case-IV: unbalanced loads supplied with unbalanced reference currents.

The current reference and load parameters for case-I to IV are chosen as:

Case-I:

$$\begin{aligned} i_a^* = i_b^* = i_c^* = 8A, \\ R_a = R_b = R_c = 6.8\Omega. \end{aligned} \quad (24)$$

Case II:

$$\begin{aligned} i_a^* = i_b^* = i_c^* = 8A, \\ R_a = 8.3\Omega, R_b = 9.6\Omega, \text{ and } R_c = 8\Omega. \end{aligned} \quad (25)$$

Case III:

$$\begin{aligned} i_a^* = 8.8A, i_b^* = 6A, i_c^* = 7.3A, \\ R_a = R_b = R_c = 8.1\Omega. \end{aligned} \quad (26)$$

Case IV:

$$\begin{aligned} i_a^* = 8.8A, i_b^* = 6A, i_c^* = 7.2A, \\ R_a = 8.6\Omega, R_b = 9.2\Omega, \text{ and } R_c = 8.2\Omega \end{aligned} \quad (27)$$

Table 2 Parameters for experimental prototype

Variable Name	Description of the variable	Unit	Value
V_{dc}	DC Link Voltage	V	200
R_s	Filter Resistance	Ω	0.01
L	Filter Inductance	mH	8
f	Fundamental Frequency	Hz	50
T_s	Sampling Period	μs	30
L_n	Neutral Point Inductance	mH	2.2

Results of Case-I presents the condition with balanced loads and balanced reference currents (Fig. 9). It is expected that a cleaner dc-supply system will give a better performance than the current one. Results of Case-II reveal unbalanced loads and balanced references in the steady-state mode (Fig. 10). This is a more practical situation when independent single-phase loads with different magnitudes connected to the inverter. It can be seen that in all the four cases the references are tracked very well underpinning the validity of the proposed predictive current control technique (Figs. 9–12). It can be observed that the controller tracks the current reference well with both balanced and unbalanced loads. Moreover, the controller is also effective to track the unbalanced current references. It is to be mentioned that the filter parameters are selected such that the total harmonic distortion (THD) value remains acceptable for real-time applications (less than 5%).

5.2 Transient performance analysis

The transient test results are shown in Fig. 13 and Fig. 14. The dynamic response of the load current is extremely fast (no overshoot and very short settling time) without any

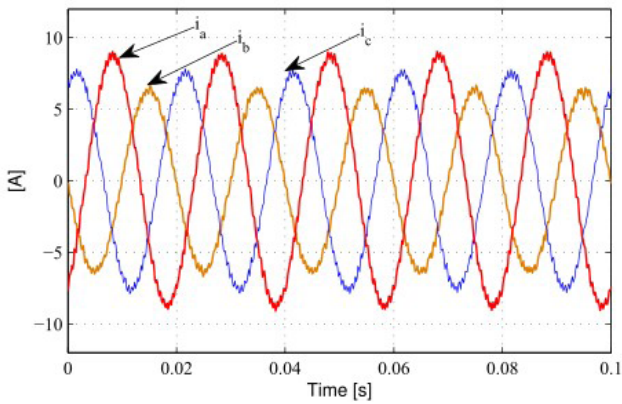


Fig. 9 Case I results: balanced load supplied with balanced reference

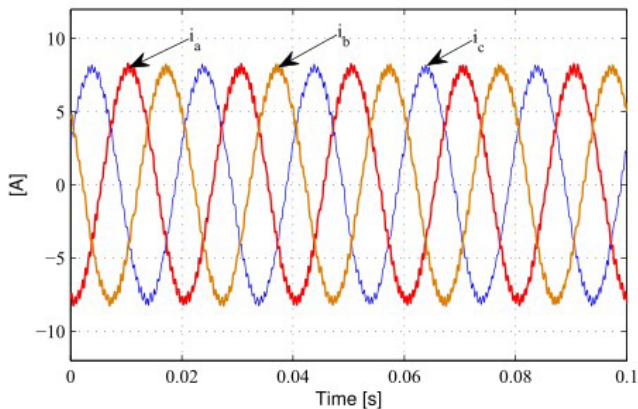


Fig. 10 Case II results: unbalanced load supplied with balanced reference currents

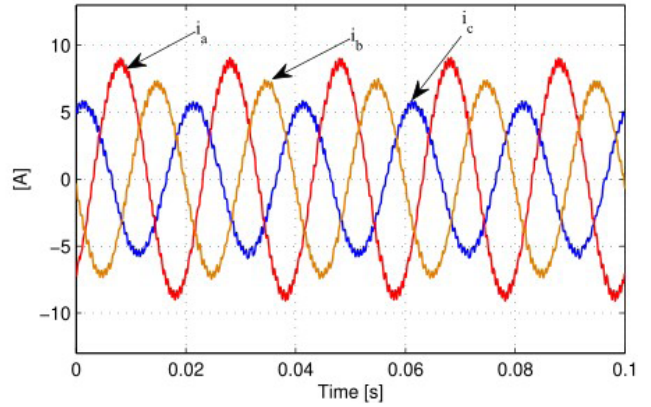


Fig. 11 Case III results: unbalanced load supplied with unbalanced reference currents

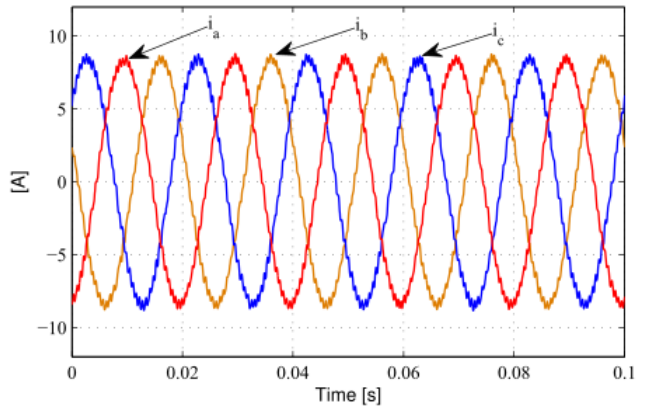


Fig. 12 Case IV results: balanced load supplied with unbalanced reference currents

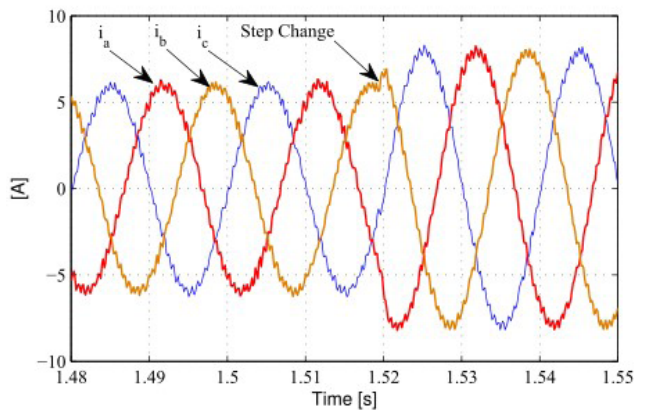


Fig. 13 Transients analysis for case I: balanced load with balanced reference currents

sacrifice in the tracking of the reference current. The proposed method with five-voltage vectors in the prediction process offers exactly same transient performance as the sixteen-voltage vector one. It has been experimentally proven that the proposed control technique can exhibit similar output performances compared to the conventional FCS-MPC scheme.

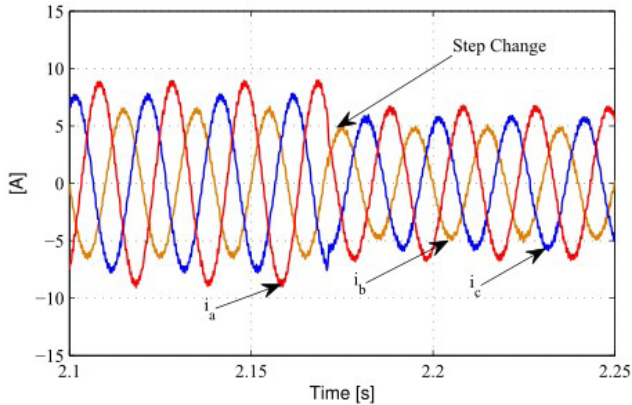


Fig. 14 Transients analysis for case III: unbalanced load with unbalanced reference currents

5.3 Evaluation of computational Burden Reduction

One of the significant concern of FCS-MPC for the four-legged inverter is a large number of calculations in the prediction loop during each sampling interval. The proposed method can reduce the execution time from 22.6- μ s to 17.9- μ s for a DS-1104 platform. The comparison among different MPC algorithm is shown in Table 3. The measurement of the computational time is achieved in DSpace real-time measurement by using the command 'RTLIB TIC START' and 'RTLIB TIC READ' in C.

5.4 Investigation on switching frequency reduction

For reducing the switching frequency effort, additional switching frequency penalization term can be added in the cost function as Eq. (28). Thus, the final cost function becomes:

$$J[k+1] = \left| \mathbf{u}_{inv}^*[k+1] - \mathbf{u}_{inv}[k+1] \right| + k_{sw} n_{sw} \quad (28)$$

k_{sw} is the weighting factor and n_{sw} is the number of commutations imposed by the switching state under evaluation.

Table 3 Comparison among different MPC algorithms

Method	Voltage Vectors	Stability	Complexity
Conventional	16	No	Low
Proposed method without preselection	16	Yes	Low
Proposed method with preselection	5	Yes	Low

The relationship between the weighting factor, the average switching frequency of the device and the THD of the load current is shown using a 3-D line plot (Fig. 15). It can be concluded that with the increased value of weighting factor the switching frequency reduction is possible, but it comes at the cost of higher ripple in the load current as illustrated in Fig. 15.

5.5 Robustness to parameter variation

As the state variables of the converter for the present analysis are being influenced by measurement errors, it is necessary to examine the robustness of the control technique against parameter variation. This subsection involves the mathematical formulation of the robustness of the proposed controller against parameter variation. This approach involves the definition of the cost function. The cost function of the proposed technique can be represented as [28]:

$$J[k+1] = \left| \mathbf{x}^*[k+1] - \mathbf{x}[k+1] \right|, \quad (29)$$

where,

$$\mathbf{x}[k+1] = \mathbf{A}\mathbf{y}[k] + \mathbf{B}\mathbf{u}[k+1] + \mathbf{D}. \quad (30)$$

Detailed description about the matrices (A, B and D) can be found in [14]. The simplified version of the cost function form the control point of view can be defined as:

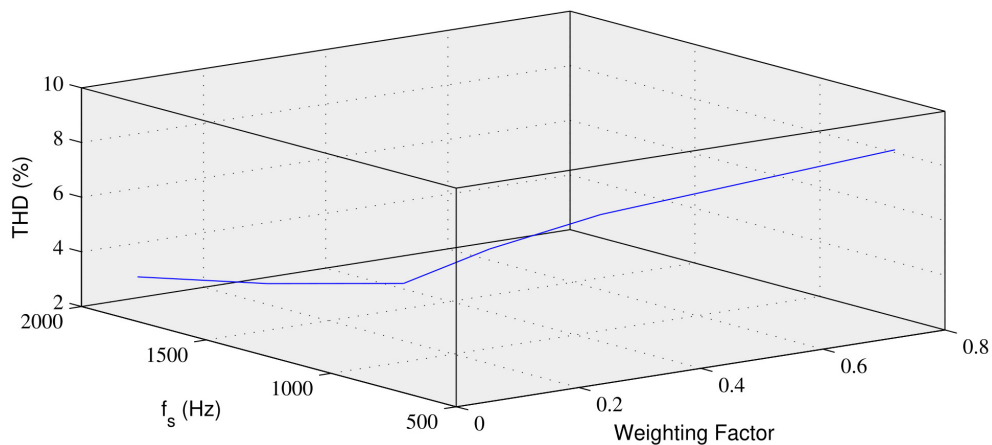


Fig. 15 3-D line plot illustrating the relationship between weighting factor, the average switching frequency of the device and THD of the load current

$$\mathbf{x}[k+1] \in \mathbf{x}_v[k+1] \text{ or } \mathbf{g}[k+1] < \mathbf{g}[k]. \quad (31)$$

Here, \mathbf{x}_v is the region of the voltage set. Now considering the additive uncertainty parameter, the following term can be derived:

$$\mathbf{x}_d[k+1] = (\mathbf{A} + \hat{\mathbf{A}})\mathbf{y}[k] + (\mathbf{B} + \hat{\mathbf{B}})\mathbf{u}[k+1] + \mathbf{D}. \quad (32)$$

Here, the \mathbf{A} and \mathbf{B} matrices correspond to the nominal response of the model, $\hat{\mathbf{A}}$ and $\hat{\mathbf{B}}$ takes into account the uncertainty of the model. Taken together the reference value of x , the equation can be written as:

$$\mathbf{x}[k+1] - \mathbf{x}^*[k+1] < \mathbf{x}[k+1] - \mathbf{x}^*[k] + \hat{\mathbf{A}}\mathbf{y}[k] + \hat{\mathbf{B}}\mathbf{u}[k+1]. \quad (33)$$

Considering the upper bound of the uncertainty the following equation can be written:

$$\mathbf{x}[k+1] - \mathbf{x}^*[k+1] + \mathbf{b}_1\mathbf{y}[k] + \mathbf{b}_2 < \mathbf{x}[k+1] - \mathbf{x}^*[k], \quad (34)$$

which is equivalent to:

$$\mathbf{J}[k+1] + \mathbf{b}_1\mathbf{y}[k] + \mathbf{b}_2 < \mathbf{J}[k]. \quad (35)$$

To ensure robust performance of the controller, in case of the variable overflow on the right hand side constraint of Eq. (31) should be modified with the objective of minimum tracking towards the set point of the current. More specifically, the constraint at $(k + 1)$ should be interchanged with $\mathbf{x}[k + 1] \forall \mathbf{r}_v$. Here, \mathbf{r}_v uses a radius ($\hat{\mathbf{r}}_v$). ($\hat{\mathbf{r}}_v$) can be expressed as [22]:

$$\hat{\mathbf{r}} = \mathbf{r}_v - \mathbf{b}_1|\mathbf{y}(k)| - \mathbf{b}_2. \quad (36)$$

Thus, the uncertainty of the \mathbf{r}_v which is defined as a $\hat{\mathbf{r}}_v$ is a subset of \mathbf{r}_v ensuring the robust behavior of the proposed approach. To verify the robustness analysis shown in the previous section, the value of the filter parameter is varied up to 100%, and it is found that the percentage current error is within the tolerance limit. Fig. 16 illustrates the variation of THD with variation of neutral inductance. One case scenario of percentage current error is shown in Fig. 17 when filter inductance is varied from 8-mH to 16-mH. Another case scenario of percentage current error is shown in Fig. 18 when filter inductance is varied from 8-mH to 12-mH. Unaware of the filter parameter variation, the controller tracking is still quite robust. However, the extreme condition of filter parameter variation may be not suitable for the controller, and thus an online estimation of the filter parameter is required. The neutral inductance (L_n) is used to reduce the switching frequency ripple in the neutral current. The results are summarized in

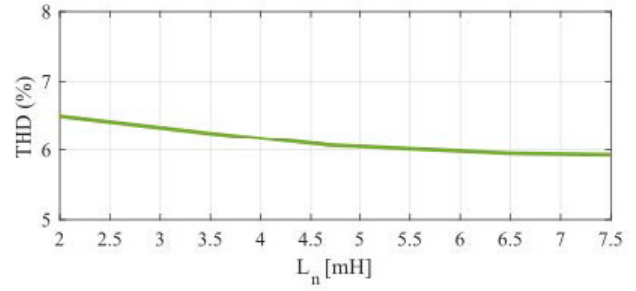


Fig. 16 Variation of THD with variation of neutral inductance

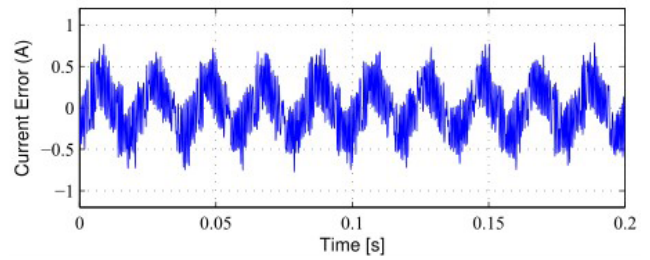


Fig. 17 Current error(%) for $L_f = 16$ mH

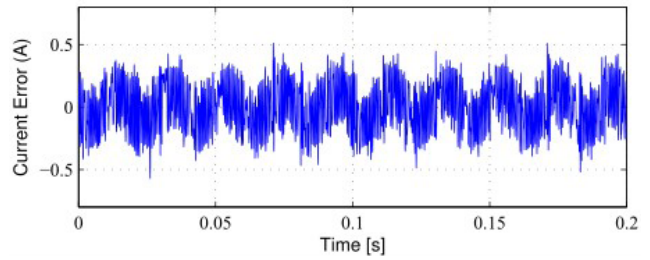


Fig. 18 Current error(%) for $L_f = 12$ mH

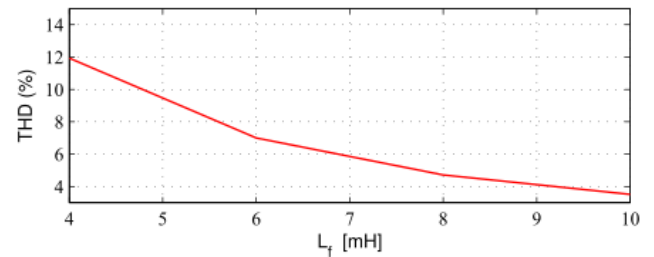


Fig. 19 Variation of THD with variation of filter inductance

Fig. 19. As expected, the lower values of the filter inductance lead to higher THD of the load current. It can be seen that the effect of varying the filter inductance is much more significant than the neutral inductance. As far as the role of a neutral inductor is concerned, without the neutral inductor or at lower values-neutral inductor the THD of the load current will be increased.

6 Conclusions

This work proposes a modified predictive control scheme for four-legged inverters, which readily ensures the global stability of the overall system. The first contribution of

this work leads to a reduction of computational burden using the preselection approach. The second contribution of this work is to investigate the stability of the overall system by using Lyapunov's direct method. Experimental results are presented to provide support to the theoretical approach. Analysis involving the robustness against

parameter variation, are also presented. Overall, experimental results demonstrate that the proposed predictive control technique offers a simplified approach that alleviates the computational effort of the controller while ensuring the global stability.

References

- [1] Kroposki, B., Johnson, B., Zhang, Y., Gevorgian, V., Denholm, P., Hodge, B.-M., Hannegan, B. "Achieving a 100% renewable grid: Operating electric power systems with extremely high levels of variable renewable energy", *IEEE Power and Energy Magazine*, 15(2), pp. 61–73, 2017.
<https://doi.org/10.1109/MPE.2016.2637122>
- [2] Golsorkhi, M. S., Lu, D. D.-C., Guerrero, J. M. "A gps-based decentralized control method for islanded microgrids", *IEEE Transactions on Power Electronics*, 32(2), pp. 1615–1625, 2017.
<https://doi.org/10.1109/TPEL.2016.2551265>
- [3] Rojas, F., Kennel, R., Cardenas, R., Repenning, R., Clare, J. C., Diaz, M. "A New Space-Vector-Modulation Algorithm for a Three-Level Four-Leg NPC Inverter", *IEEE Transactions Energy Conversion*, 32(1), pp. 23–35, 2017.
<https://doi.org/10.1109/TEC.2016.2605076>
- [4] Basri, H. M., Mekhilef, S. "Digital predictive current control of multi-level fourleg voltage-source inverter under balanced and unbalanced load conditions", *IET Electric Power Applications*, 11(8), pp. 1499–1508, 2017.
<https://doi.org/10.1049/iet-epa.2017.0032>
- [5] Lidozzi, A., Solero, L., Bifaretti, S., Crescimbin, F. "Sinusoidal voltage shaping of inverter-equipped stand-alone generating units", *IEEE Transactions on Industrial Electronics*, 62(6), pp. 3557–3568, 2015.
<https://doi.org/10.1109/TIE.2014.2370939>
- [6] Ebrahimzadeh, E., Farhangi, S., Iman-Eini, H., Blaabjerg, F. "Modulation technique for Four-Leg Voltage Source Inverter without a Look-Up Table", *IET Power Electronics*, 9(4), pp. 648–656, 2016.
<https://doi.org/10.1049/iet-pel.2015.0310>
- [7] Guo, X., He, R., Jian, J., Lu, Z., Sun, X., Guerrero, J. M. "Leakage Current Elimination of Four-Leg Inverter for Transformerless Three-Phase PV Systems", *IEEE Transactions on Power Electronics*, 31(3), pp. 1841–1846, 2016.
<https://doi.org/10.1109/TPEL.2015.2477539>
- [8] Singh, M., Khadkikar, V., Chandra, A., Varma, R. K. "Grid interconnection of renewable energy sources at the distribution level with power-quality improvement features", *IEEE Transactions on Power Delivery*, 26(1), pp. 307–315, 2011.
<https://doi.org/10.1109/TPWRD.2010.2081384>
- [9] Zhang F., Yan, Y. "Selective harmonic elimination PWM control scheme on a three-phase four-leg voltage source inverter", *IEEE Transactions on Power Electronics*, 24(7), pp. 1682–1689, 2009.
<https://doi.org/10.1109/TPEL.2009.2014378>
- [10] Dai, N.-Y., Wong, M.-C., Ng, F., Han, Y.-D. "A FPGA-based generalized pulse width modulator for three-leg center-split and four-leg voltage source inverters", *IEEE Transactions on Power Electronics*, 23(3), pp. 1472–1484, 2008.
<https://doi.org/10.1109/TPEL.2008.921103>
- [11] Zhang, R., Prasad, V., Boroyevich, D., Lee, F. "Three-dimensional space vector modulation for four-leg voltage-source converters", *IEEE Transactions on Power Electronics*, 17(3), pp. 314–326, 2002.
<https://doi.org/10.1109/TPEL.2002.1004239>
- [12] Pichan, M., Rastegar, H. "Sliding-Mode Control of Four-Leg Inverter With Fixed Switching Frequency for Uninterruptible Power Supply Applications", *IEEE Transactions on Industrial Electronics*, 64(8), pp. 6805–6814, 2017.
<https://doi.org/10.1109/TIE.2017.2686346>
- [13] Pichan, M., Rastegar, H., Monfared, M. "Deadbeat Control of the Stand-Alone Four-Leg Inverter Considering the Effect of the Neutral Line Inductor", *IEEE Transactions on Industrial Electronics*, 64(4), pp. 2592–2601, 2017.
<https://doi.org/10.1109/TIE.2016.2631459>
- [14] Rivera, M., Yaramasu, V., Llor, A., Rodriguez, J., Wu, B., Fadel, M. "Digital Predictive Current Control of a Three-Phase Four-Leg Inverter", *IEEE Transactions on Industrial Electronics*, 60(11), pp. 4903–4912, 2013.
<https://doi.org/10.1109/TIE.2012.2219837>
- [15] Yaramasu, V., Rivera, M., Narimani, M., Wu, B., Rodriguez, J. "Model Predictive Approach for a Simple and Effective Load Voltage Control of Four-Leg Inverter with an Output LC Filter", *IEEE Transactions on Industrial Electronics*, 61(10), pp. 5259–5270, 2014.
<https://doi.org/10.1109/TIE.2013.2297291>
- [16] Bayhan, S., Trabelsi, M., Abu-Rub, H., Malinowski, M. "Finite-Control-Set Model-Predictive Control for a Quasi-Z-Source Four-Leg Inverter Under Unbalanced Load Condition", *IEEE Transactions on Industrial Electronics*, 64(4), pp. 2560–2569, 2017.
<https://doi.org/10.1109/TIE.2016.2632062>
- [17] Yaramasu, V., Rivera, M., Wu, B., Rodriguez, J. "Model predictive current control of two-level four-leg inverters Part I: Concept algorithm and simulation analysis", *IEEE Transactions on Power Electronics*, 28(7), pp. 3459–3468, 2013.
<https://doi.org/10.1109/TPEL.2012.2227509>
- [18] Yaramasu, V., Wu, B., Rivera, M., Rodriguez, J., Wilson, A. "Cost function based predictive voltage control of two-level four-leg inverters using two step prediction horizon for standalone power systems", In: 2012 Twenty-Seventh Annual IEEE Applied Power Electronics Conference and Exposition (APEC), Orlando, FL, USA, 2012, pp. 128–135. ISBN 978-1-4577-1215-9
<https://doi.org/10.1109/APEC.2012.6165808>
- [19] Chen, Q., Luo, X., Zhang, L., Quan, S. "Model Predictive Control for ThreePhase Four-Leg Grid-Tied Inverters", *IEEE Access*, 5, pp. 2834–2841, 2017.
<https://doi.org/10.1109/ACCESS.2017.2664983>

- [20] Vatani, M., Hovd, M. "Lyapunov-based proportional-integral controller design with guaranteed region of convergence for dc-dc power converters", In: 2017 12th IEEE Conference on Industrial Electronics and Applications (ICIEA), Siem Reap, Cambodia, 2017, pp. 1443–1448. ISBN 978-1-5090-6162-4
<https://doi.org/10.1109/ICIEA.2017.8283066>
- [21] Bariša, T., Ileš, Š., Sumina, D., Matuško, J. "Model Predictive Direct Current Control of a Permanent Magnet Synchronous Generator Based on Flexible Lyapunov Function Considering Converter Dead Time", IEEE Transactions on Industry Applications, 54(3), pp. 2899–2912, 2018.
<https://doi.org/10.1109/TIA.2018.2801838>
- [22] Parvez Akter, M., Mekhilef, S., Tan, N. M. L., Akagi, H. "Modified Model Predictive Control of a Bidirectional AC–DC Converter Based on Lyapunov Function for Energy Storage Systems", IEEE Transactions on Industrial Electronics, 63(2), pp. 704–715, 2016.
<https://doi.org/10.1109/TIE.2015.2478752>
- [23] Aguilera, R. P., Quevedo, D. E. "Predictive Control of Power Converters: Designs With Guaranteed Performance", IEEE Transactions on Industrial Informatics, 11(1), pp. 53–63, 2015.
<https://doi.org/10.1109/TII.2014.2363933>
- [24] Wi, S.-M., Lee, J. S., Kim, M. "Exponentially Stable Lyapunov-Function-Based Controller for a Flyback CCM Converter", IEEE Transactions on Industrial Electronics, 65(2), pp. 1213–1225, 2018.
<https://doi.org/10.1109/TIE.2017.2733459>
- [25] Beiranvand, H., Rokrok, E. "Asymptotically stable controller for SSTs based on Lyapunov direct stability method", IET Power Electronics, 10(5), pp. 2065–2075, 2017.
<https://doi.org/10.1049/iet-pel.2017.0285>
- [26] Sefa, I., Ozdemir, S., Komurcugil, H., Altin, N. "Comparative study on Lyapunov-function-based control schemes for single-phase grid-connected voltage-source inverter with LCL filter", IET Renewable Power Generation, 11(11), pp. 1473–1482, 2017.
<https://doi.org/10.1049/iet-rpg.2016.0566>
- [27] Pepe, P. "On Control Lyapunov–Razumikhin Functions, Nonconstant Delays, Nonsmooth Feedbacks, and Nonlinear Sampled-Data Stabilization", IEEE Transactions on Automatic Control, 62(11), pp. 5604–5619, 2017.
<https://doi.org/10.1109/TAC.2017.2689500>
- [28] Geyer, T., Aguilera, R. P., Quevedo, D. E. "On the stability and robustness of model predictive direct current control", In: 2013 IEEE International Conference on Industrial Technology (ICIT), Cape Town, South Africa, 2013, pp. 374–379. ISBN 978-1-4673-4567-5
<https://doi.org/10.1109/ICIT.2013.6505701>
- [29] Aguilera, R. P., Quevedo, D. E. "On stability and performance of finite control set MPC for power converters", In: 2011 Workshop on Predictive Control of Electrical Drives and Power Electronics, Munich, Germany, 2011, pp. 55–62. ISBN 978-1-4577-1912-7
<https://doi.org/10.1109/PRECEDE.2011.6078688>